

## Magnetic phase transitions in $\text{Pr}_5\text{Ge}_4$

G. H. Rao,<sup>1,2</sup> Q. Huang,<sup>2</sup> H. F. Yang,<sup>1</sup> D. L. Ho,<sup>2</sup> J. W. Lynn,<sup>2</sup> and J. K. Liang<sup>1</sup>  
<sup>1</sup>*Institute of Physics and Center for Condensed Matter Physics, Chinese Academy of Sciences,  
 Beijing 100080, People's Republic of China*

<sup>2</sup>*NIST Center for Neutron Research, National Institute of Standards and Technology,  
 Gaithersburg, Maryland 20899-8562, USA*

(Received 18 November 2003; revised manuscript received 22 January 2004; published 25 March 2004)

The magnetic structure and magnetic phase transitions of the  $\text{Pr}_5\text{Ge}_4$  compound are investigated by means of neutron powder diffraction (NPD) and small-angle neutron scattering (SANS). Both NPD and SANS indicate the existence of two magnetic phase transitions at 25 K and 42 K. Refinement of the crystal structure based on the high-resolution NPD data shows that from room temperature to 1.6 K the compound maintains the  $\text{Sm}_5\text{Ge}_4$ -type structure ( $Pnma$ ,  $Z=4$ ), in which Ge atoms occupy two  $4c$  sites and one  $8d$  site and Pr atoms occupy two  $8d$  sites and one  $4c$  site. Refinements of the magnetic structures reveal that the two magnetic transitions essentially correspond to the long-range orderings of the Pr moments on different crystallographic sites. The Pr moments on the  $4c$  site order ferromagnetically with  $Pn'm'a'$  symmetry at 42 K and induce small ordered Pr moments on the  $8d$  sites. The long-range ordering of the Pr moments on the  $8d$  sites develops at 25 K with  $Pnm'a'$  symmetry. The separate ordering of the Pr moments on different crystallographic sites can be readily understood by the salient difference in the rare earth metal environments between the different crystallographic sites. The Pr moments on the  $4c$  site in  $\text{Pr}_5\text{Ge}_4$  compound align along the  $b$  axis, in contrast to other reported  $R_5\text{Ge}_4$  compounds, and can be attributed to the contribution of higher-order terms of crystal-field to magnetocrystalline anisotropy of the various  $R$  atoms in the  $R_5\text{Ge}_4$  compounds.

DOI: 10.1103/PhysRevB.69.094430

PACS number(s): 75.25.+z, 75.30.Kz, 75.50.Cc

### I. INTRODUCTION

Interest in the  $R_5(\text{Si,Ge})_4$  pseudobinary alloys ( $R$ =rare earth) has been revived recently owing to the discovery of a giant magnetocaloric effect (MCE) in  $\text{Gd}_5(\text{Si}_{1-x}\text{Ge}_x)_4$  by Pecharsky and Gschneidner,<sup>1,2</sup> which is attractive for its potential application as magnetic refrigerants. The giant MCE in  $\text{Gd}_5(\text{Si}_{1-x}\text{Ge}_x)_4$  shows a maximum at a specific temperature tunable by adjusting the Ge content<sup>2</sup> and is essentially due to simultaneous first-order structural/magnetic phase transitions near that temperature.<sup>3,4</sup> These transitions also lead to a strong magnetoelastic effect<sup>3</sup> and giant magnetoresistance<sup>5</sup> of the compounds. Similar effects were observed in other  $R_5(\text{Si,Ge})_4$  alloys<sup>6,7</sup> and recently in  $\text{Gd}_5\text{Sn}_4$ .<sup>8</sup> Knowledge of the magnetic structures of these compounds is indispensable for understanding these intriguing field-dependent properties of the compounds. However, such knowledge remains largely unknown, although  $R_5\text{Si}_4$  and  $R_5\text{Ge}_4$  compounds were discovered and their crystal structures were identified over 30 years ago.<sup>9</sup>

$R_5\text{Si}_4$  crystallizes in either the tetragonal  $\text{Zr}_5\text{Si}_4$ -type structure (space group  $P4_12_12$ ) or the orthorhombic  $\text{Gd}_5\text{Si}_4$ -type structure (space group  $Pnma$ ) depending on whether  $R$  is a light or a heavy rare earth metal, whereas all  $R_5\text{Ge}_4$  compounds crystallize in the orthorhombic  $\text{Sm}_5\text{Ge}_4$ -type structure (space group  $Pnma$ ).<sup>9,10</sup> The structures of  $\text{Gd}_5\text{Si}_4$  and  $\text{Gd}_5\text{Ge}_4$  as well as their difference were nicely illustrated by Pecharsky and Gschneidner.<sup>11</sup> Both structures are basically built from equivalent layers (slabs) that are infinite in two dimensions ( $a$  and  $c$ ). The Gd atom on the  $4c$  site is coordinated by six Si or Ge atoms forming a distorted octahedron and by eight Gd atoms on two differ-

ent  $8d$  sites (four on each  $8d$  site) forming a slightly distorted cube that shares edges with each other to form the slab. The Si or Ge atoms inside the slab form partially covalent bonds, and the other Si or Ge atoms locate on the surface of the slab. In  $\text{Gd}_5\text{Si}_4$  the slabs are all interconnected via partially covalent interslab Si-Si bonds, while in  $\text{Gd}_5\text{Ge}_4$  all the interslab Ge-Ge bonds are broken.<sup>12</sup> For the purpose of constructing a magnetic structure model, only the magnetic rare earth atoms are considered, and the structure can be viewed as composed of two-dimensional slabs consisting of the edge-shared cubes and interconnected by shorter bonds between  $R$  atoms on two different  $8d$  sites. Figure 1 illustrates the crystal structure of  $\text{Pr}_5\text{Ge}_4$ .

The magnetic structures of only a few  $R_5\text{Ge}_4$  compounds were studied by neutron diffraction—i.e.,  $\text{Tb}_5\text{Ge}_4$ ,<sup>13</sup>  $\text{Ho}_5\text{Ge}_4$ ,<sup>14</sup> and  $\text{Nd}_5\text{Ge}_4$ .<sup>15</sup> Recently the magnetic structures of  $\text{Tb}_5(\text{Si}_x\text{Ge}_{1-x})_4$  were investigated by Ritter *et al.*<sup>16</sup> and those of  $\text{Nd}_5\text{Si}_4$  and  $\text{Nd}_5\text{Ge}_4$  by Cadogan *et al.*<sup>17</sup> It is intriguing to notice that, unlike the crystal structure, the magnetic structures of  $R_5\text{Ge}_4$  belong to different magnetic space groups depending on the rare earth—e.g.,  $Pnm'a'$  for  $\text{Tb}_5\text{Ge}_4$ ,  $Pn'm'a'$  for  $\text{Ho}_5\text{Ge}_4$ , and  $Pnm'a'$  for  $\text{Nd}_5\text{Ge}_4$ . In addition, neutron diffraction studies reveal that there are two magnetic phase transitions in  $\text{Ho}_5\text{Ge}_4$  and  $\text{Tb}_5\text{Ge}_4$ . Two magnetic phase transitions are also evident in  $\text{Pr}_5\text{Ge}_4$  in the temperature dependence of the magnetization in a field of 500 Oe.<sup>18</sup> As temperature increases, the magnetization curve exhibits two sudden drops at  $T_C^I=25$  K and  $T_C^{II}=41$  K, respectively. A large magnetoresistance ( $\Delta\rho/\rho$ ) was observed (about 25% at 24 K and 15% at 40 K) in the presence of a magnetic field of 5 T.

$\text{Pr}_5\text{Ge}_4$  crystallizes in the  $\text{Sm}_5\text{Ge}_4$  structure. Detailed crystallographic data, including lattice parameters, atomic positions, and bond lengths derived from x-ray powder dif-

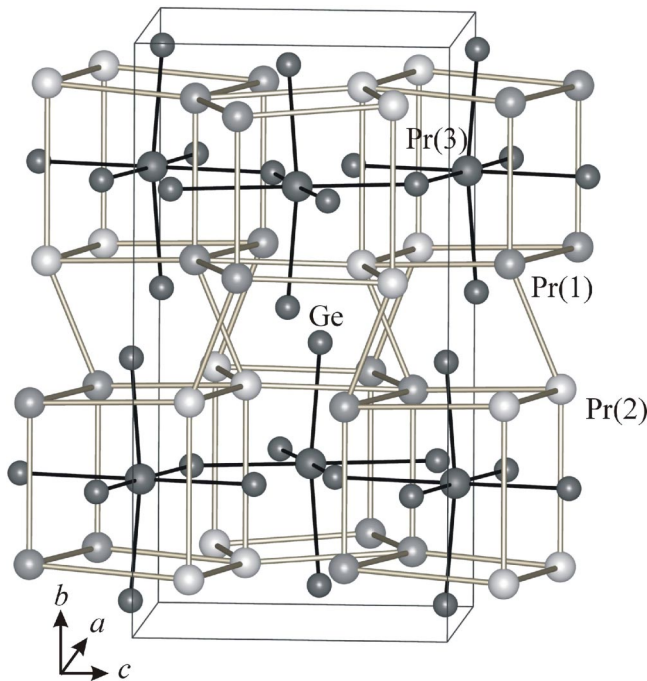


FIG. 1. Crystal structure of  $\text{Pr}_5\text{Ge}_4$ . Small and larger balls stand for Ge and Pr atoms, respectively. The bonding between Ge and Pr at the  $4c$  site (Pr3) and the coordination cube of Pr atoms around the Pr atom at the  $4c$  site are illustrated. Pr1 and Pr2 denote Pr atoms located on the two different  $8d$  sites.

fraction (XRD) data, were reported by Yang *et al.*<sup>19</sup> In the present work we focus on the investigation of the magnetic structure of  $\text{Pr}_5\text{Ge}_4$  by means of temperature-dependent small-angle neutron scattering (SANS) and neutron powder diffraction (NPD).

## II. EXPERIMENT

The sample of polycrystalline  $\text{Pr}_5\text{Ge}_4$  was prepared by arc-melting the mixture of pure metal components (with purity better than 99.9% for Pr and 99.9999% for Ge from General Research Institute for Nonferrous Metals, China) in a water-cooled copper hearth under an argon atmosphere as described previously.<sup>18,19</sup> All the neutron experiments were performed at the NIST Center for Neutron Research (NCNR). SANS measurements over the  $q$  range from  $0.008 \text{ \AA}^{-1}$  to  $0.132 \text{ \AA}^{-1}$  were carried out using the NG-1 8-m SANS instrument with an incident neutron wavelength of  $\lambda = 8 \text{ \AA}$  and resolution of  $\Delta\lambda/\lambda = 0.14$ . The magnetic order parameter and coarse-resolution magnetic diffraction patterns were determined on the BT-7 spectrometer with a wavelength of  $2.4649 \text{ \AA}$ . NPD data for refinement of the magnetic structures were collected on the high-resolution, 32-counter BT-1 diffractometer. A Cu(311) monochromator was used to produce a monochromatic neutron beam of wavelength  $1.5402(1) \text{ \AA}$ . Collimators with horizontal divergence of  $15'$ ,  $20'$ , and  $7'$  full width at half maximum of arc were used before and after the monochromator and after the sample, respectively. Data were collected in the  $2\theta$  range of

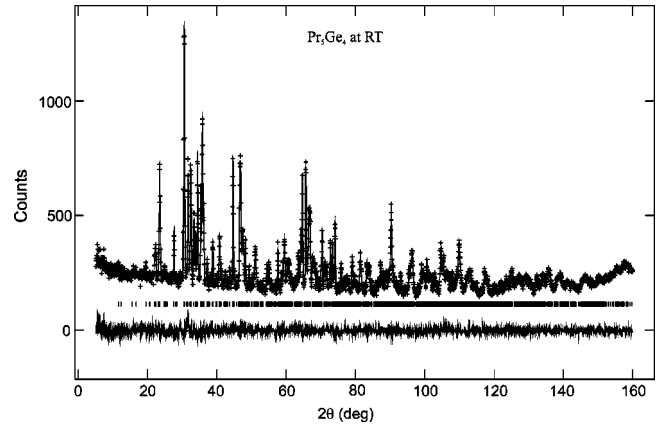


FIG. 2. Observed (crosses) and calculated (solid line) intensities for  $\text{Pr}_5\text{Ge}_4$  at 295 K. Differences are shown at bottom of the figure. The vertical bars indicate the Bragg positions.

$3^\circ$ – $168^\circ$  with a step of  $0.05^\circ$ . The structure refinements were carried out using the program GSAS.<sup>20</sup>

## III. RESULTS AND DISCUSSION

Neutron diffraction at room temperature confirms the investigated  $\text{Pr}_5\text{Ge}_4$  to be paramagnetic and to crystallize in the  $\text{Sm}_5\text{Ge}_4$ -type structure ( $Pnma$ ,  $Z=4$ ). The derived lattice constants from the structure refinement are  $a = 7.9172(4) \text{ \AA}$ ,  $b = 15.1916(7) \text{ \AA}$ , and  $c = 8.0112(4) \text{ \AA}$ , in good agreement with the XRD results.<sup>9,19</sup> No structural transitions were detected between 9 and 295 K.

Figure 2 shows the experimental and calculated NPD patterns of the  $\text{Pr}_5\text{Ge}_4$  compound at room temperature. The refined structural parameters and  $R$  factors of the refinement for  $\text{Pr}_5\text{Ge}_4$  are listed in Table I.

Figure 3 shows the magnetic diffraction patterns obtained by subtracting the data at 26 and 9 K, respectively, from the data taken at 60 K, well above the magnetic ordering temperature. The magnetic Bragg peaks can be indexed on the nuclear unit cell. The temperature dependence of the peak intensity of the overlapping (131) and (040) peaks and the integrated intensity of the (010) peak measured on BT-7 during warming are shown in Fig. 4(a). The temperature dependence of the peak intensity of the (131) overlapping the (040) peak is very similar to the low-field magnetization curve reported in Ref. 18. Two steps are evident: one occurs at  $\sim 25 \text{ K}$  and the other at  $\sim 42 \text{ K}$ . Both temperatures coincide well with the magnetic transition temperatures derived from the magnetization measurements. The (010) peak is a purely magnetic one, and on warming its integrated intensity starts to appear at about 15 K when the (131) and (040) peak intensities begin to decrease prominently. The intensity increases rapidly, reaches a maximum at about 32 K where the lower step of the (131) and (040) peak intensities obviously decline. The (010) peak then disappears at the magnetic transition temperature  $T_C^{\text{II}} = 41 \text{ K}$ .<sup>18</sup> The evolution of the magnetic (010) peak strongly suggests a change of symmetry of the magnetic structure.

Small-angle neutron scattering is particularly sensitive to the ferromagnetic component of a magnetic structure, and

TABLE I. Crystallographic data and magnetic moments of Pr<sub>5</sub>Ge<sub>4</sub> at room temperature, 50 K, 30 K, and 9 K derived from refinements of the high-resolution neutron diffraction data.  $x, y, z$  are fractional coordinates of the atoms in a unit cell,  $U_{\text{iso}}$  is the isotropic temperature factor, and  $\mu_x, \mu_y, \mu_z$  are components of the magnetic moment along the  $a, b, c$  directions, respectively.  $R_p$  and  $R_{\text{wp}}$  are residuals of fitting to the pattern and weighted pattern, respectively.  $\chi^2$  is a “goodness of fit” indicator (Ref. 20).

	9 K <sup>a</sup>	9 K	30 K	50 K	Room temperature
$a$ (Å)	7.9099(2)	7.9105(2)	7.9114(2)	7.9117(3)	7.9172(4)
$b$ (Å)	15.1441(5)	15.1455(3)	15.1404(3)	15.1409(7)	15.1916(7)
$c$ (Å)	7.9968(3)	7.9973(3)	7.9966(2)	7.9943(3)	8.0112(4)
$V$ (Å <sup>3</sup> )	957.92(7)	958.15(4)	957.84(3)	957.64(7)	963.55(8)
Ge (4c): $x$	0.9088(4)	0.9096(4)	0.9102(4)	0.9098(4)	0.9121(4)
$y$	1/4	1/4	1/4	1/4	1/4
$z$	0.1081(4)	0.1078(4)	0.1075(4)	0.1083(4)	0.1079(4)
$100U_{\text{iso}}$	0.33(7)	0.58(7)	0.53(7)	0.44(8)	0.92(7)
Ge (4c): $x$	0.1781(4)	0.1786(4)	0.1784(4)	0.1771(4)	0.1784(4)
$y$	1/4	1/4	1/4	1/4	1/4
$z$	0.6300(4)	0.6300(4)	0.6308(4)	0.6313(4)	0.6313(4)
$100U_{\text{iso}}$	0.16(7)	0.17(7)	0.28(7)	0.26(8)	1.07(8)
Ge (8d): $x$	0.2224(3)	0.2222(3)	0.2228(3)	0.2224(3)	0.2209(3)
$y$	0.9541(1)	0.9541(1)	0.9546(1)	0.9547(2)	0.9554(2)
$z$	0.5291(3)	0.5291(3)	0.5296(3)	0.5304(3)	0.5320(3)
$100U_{\text{iso}}$	0.22(5)	0.34(4)	0.24(5)	0.25(5)	0.99(5)
Pr(1) (8d): $x$	0.1163(4)	0.1164(4)	0.1158(4)	0.1166(5)	0.1196(5)
$y$	0.1139(2)	0.1141(2)	0.1143(3)	0.1139(3)	0.1147(3)
$z$	0.3376(5)	0.3368(5)	0.3372(5)	0.3375(5)	0.3370(5)
$100U_{\text{iso}}$	0.0	0.0	0.04(8)	0.40(9)	0.90(9)
$\mu_x$ ( $\mu_B$ )	2.50(6)	2.40(6)	0.61(6)		
$\mu_y$ ( $\mu_B$ )	0.33(5)	0.40(5)	0.58(7)		
$\mu_z$ ( $\mu_B$ )	-0.79(5)	-0.87(5)	-0.44(13)		
$\mu$ ( $\mu_B$ )	2.64(6)	2.58(5)	0.95(8)		
Pr(2) (8d): $x$	0.9721(5)	0.9717(4)	0.9726(5)	0.9745(5)	0.9787(5)
$y$	0.1007(2)	0.1006(2)	0.1003(2)	0.1008(3)	0.1007(3)
$z$	0.8192(5)	0.8195(5)	0.8202(5)	0.8201(5)	0.8190(6)
$100U_{\text{iso}}$	0.0	0.0	0.21(8)	0.12(9)	0.89(9)
$\mu_x$ ( $\mu_B$ )	2.26(5)	2.13(5)	-0.11(6)		
$\mu_y$ ( $\mu_B$ )	-0.33(5)	-0.40(5)	0.26(9)		
$\mu_z$ ( $\mu_B$ )	1.42(5)	1.48(5)	-0.16(14)		
$\mu$ ( $\mu_B$ )	2.69(6)	2.63(5)	0.32(11)		
Pr(3) (4c): $x$	0.2860(7)	0.2860(7)	0.2862(7)	0.2855(8)	0.2870(9)
$y$	1/4	1/4	1/4	1/4	1/4
$z$	-0.0005(6)	-0.0004(6)	0.0020(5)	0.0041(6)	0.0022(7)
$100U_{\text{iso}}$	0.0	0.0	0.26(10)	0.08(11)	1.07(12)
$\mu_x$ ( $\mu_B$ )	0.50(7)	0.0	0.0		
$\mu_y$ ( $\mu_B$ )	2.69(7)	2.66(7)	2.71(7)		
$\mu_z$ ( $\mu_B$ )	-0.28(8)	0.0	0.0		
$\mu$ ( $\mu_B$ )	2.75(7)	2.66(7)	2.71(7)		
$R_p(\%)/R_{\text{wp}}(\%)/\chi^2$	3.83/4.56/1.048	4.21/4.70/1.083	3.55/4.13/0.945	4.15/4.67/0.948	3.51/4.07/0.885

<sup>a</sup>Refinement results of the magnetic structural model with symmetry  $P112'_1/a'$ , in which the Pr atoms on the 8d site ( $x, y, z$ ) in  $Pnma$  are split into two 4e sites in  $P112'_1/a$ : ( $x, y, z$ ) and ( $x, -y + 1/2, z$ ) with moments ( $\mu_x, \mu_y, \mu_z$ ) and ( $\mu_x, -\mu_y, \mu_z$ ), respectively, whereas the Pr on the 4c site in  $Pnma$  occupy the 4e site in  $P112'_1/a$  with fixed  $y = 1/4$  and its moment follows the  $P112'_1/a'$  symmetry (see text). For the sake of comparison, the site symbol 8d is retained in the table.

Fig. 4(b) shows the temperature dependence of the SANS intensity at two selected wave vectors of  $q = 0.0102 \text{ \AA}^{-1}$  and  $q = 0.0875 \text{ \AA}^{-1}$ . The data for  $q = 0.0102 \text{ \AA}^{-1}$  exhibit two steps in agreement with the magnetization data<sup>18</sup> as well as

the results from the (131) and (040) peak intensities [Fig. 4(a)]. Two peaks are evident for the  $q = 0.0875 \text{ \AA}^{-1}$  data at  $\sim 25 \text{ K}$  and  $\sim 42 \text{ K}$ , respectively, suggestive of a spin fluctuation at the magnetic phase transitions. A sharp increase of

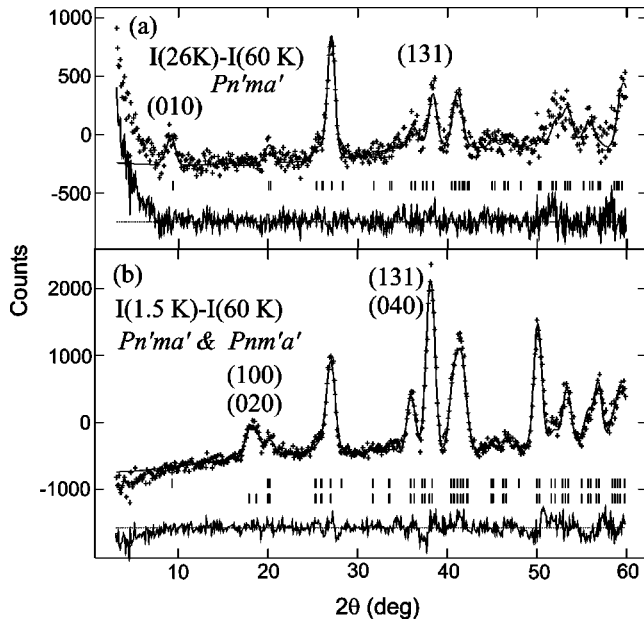


FIG. 3. Magnetic diffraction pattern (crosses) observed at (a) 26 and (b) 9 K, with good fits (solid line) using magnetic structural models of  $Pn'ma'$  and  $Pn'ma' + Pnm'a'$ . Differences between observed and calculated intensities are shown at the bottom of each figure, and the Bragg peak positions are indicated by vertical bars. Data were collected on the BT7 triple-axis diffractometer.

the ferromagnetic intensity below 25 K observed in the  $q = 0.0102 \text{ \AA}^{-1}$  curve likely originates from domain or domain wall scattering.<sup>21</sup>

The magnetic structures of  $\text{Pr}_5\text{Ge}_4$  at 30 K and 9 K were modeled successfully based on an analyses of the high-

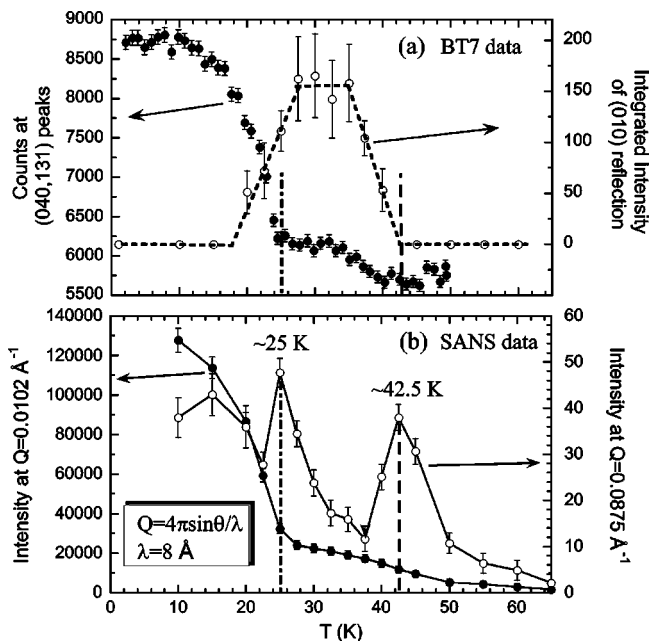


FIG. 4. (a) (131) and (040) magnetic Bragg peak intensities (solid circles) and the (010) integrated intensity (open circles, BT7 data) and (b) SANA data at  $q = 0.0102 \text{ \AA}^{-1}$  (solid circles) and  $0.0875 \text{ \AA}^{-1}$  (open circles) as a function of temperature.

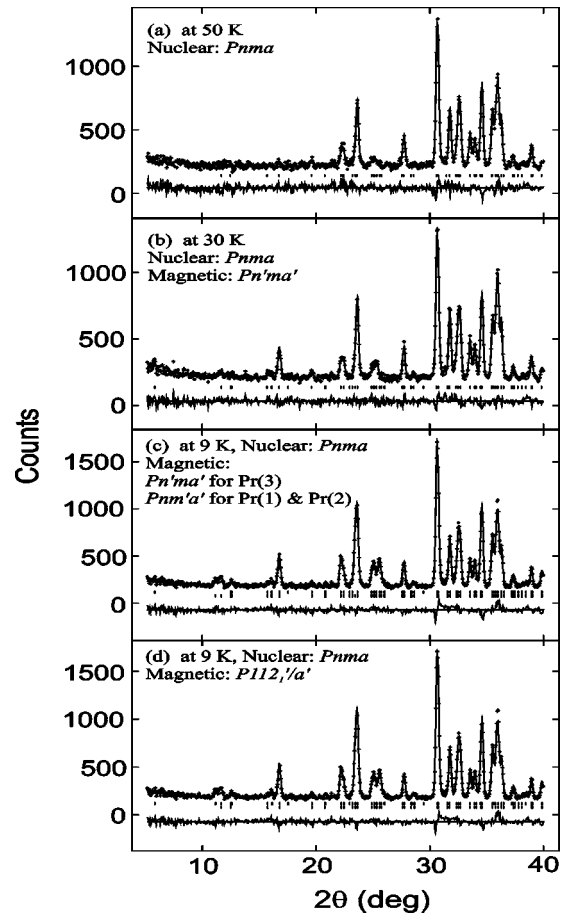


FIG. 5. Portion of the observed and calculated NPD patterns (BT1 data) in the low-angle region. (a) Nuclear fit only. (b) Both nuclear and magnetic ( $Pn'ma'$ ) fits at 30 K. (c) Both nuclear and magnetic fits at 9 K. Vertical bars indicate the Bragg peak positions for nuclear and magnetic symmetry  $Pnm'a'$  for Pr1 and Pr2 at the  $8d$  site (lower) and the magnetic symmetry  $Pn'ma'$  for Pr3 at the  $4c$  site (upper). (d) Fit with nuclear (positions of lower vertical bars) and magnetic symmetry  $P112'/a'$  (positions of upper vertical bars).

resolution NPD data. The lower-angle portions of the observed and calculated NPD patterns at 50, 30, and 9 K are shown in Fig. 5. The crystallographic data and magnetic moments of the Pr atoms are listed in Table I.

Figure 6 shows the magnetic structure models for  $\text{Pr}_5\text{Ge}_4$  at 30 and 9 K. For the sake of clarity only the Pr atoms are depicted. At 30 K, the proposed magnetic structure complies with the Shubnikov space group  $Pn'ma'$ . The magnetic moments of Pr on the  $4c$  site (Pr3) are arranged ferromagnetically along the  $b$  direction with an atomic moment of  $2.71(7)\mu_B$ , a little smaller than the theoretical value for a free trivalent ion ( $= 3.2\mu_B$ ). The reduced moment is probably due to crystal field effects (CFE's). The three components of the moment ( $\mu_x, \mu_y, \mu_z$ ) of the Pr on each  $8d$  site (Pr1 and Pr2) are comparable. The sublattice of the  $8d$  site Pr1 (or Pr2) exhibits a canted magnetic structure in the  $ac$  plane and couples antiferromagnetically (AFM) with the nearest Pr1 (or Pr2) atoms along the  $b$  direction, which makes a significant contribution to the (010) Bragg peak as

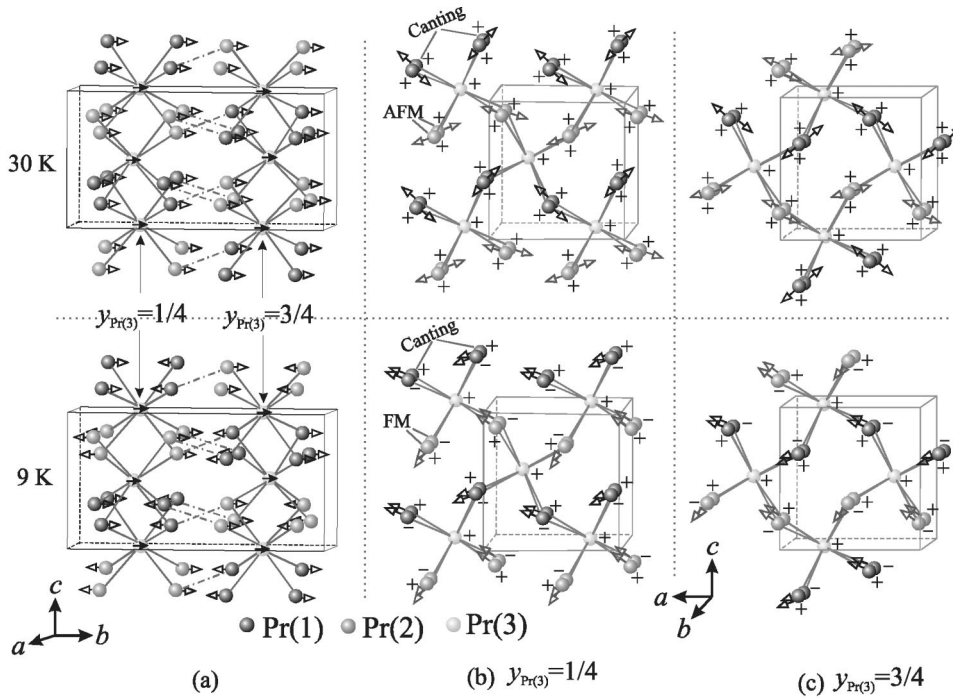


FIG. 6. Magnetic structure models for Pr<sub>5</sub>Ge<sub>4</sub> at 30 and 9 K. (a) Arrangements of the *b* components (arrows) of the Pr magnetic moments. (b) and (c) Arrangements of the Pr magnetic components in the *ac* plane (arrows) and *b* components (+ and -).

shown in Figs. 3 and 4. However, the total atomic moments are  $0.95(7)\mu_B$  and  $0.3(1)\mu_B$  for Pr1 and Pr2, respectively, much smaller than the theoretical value for a free trivalent Pr ion. As we discuss below, such small Pr moments on the 8*d* sites are probably indicative of moments that are induced by the long-range ordering of the Pr moments on the 4*c* site. This scenario is consistent with the considerable diffuse scattering at low angles at intermediate temperature in comparison to the low-temperature data (see Fig. 3). Recently, Morrell *et al.* reported a monoclinic ferromagnetic phase in Tb<sub>5</sub>Si<sub>2</sub>Ge<sub>2</sub> compound, in which the moments of Tb2A and Tb3A are much smaller than that of Tb1.<sup>22</sup> Considering that in the monoclinic structure the chemical environments of Tb2A and Tb3A in monoclinic Tb<sub>5</sub>Si<sub>2</sub>Ge<sub>2</sub> are similar to those of Pr1 and Pr2 in Pr<sub>5</sub>Ge<sub>4</sub>, while the chemical environment of Tb1 is similar to that of Pr3, it is reasonable to attribute the diminished magnetic moments of Tb2A and Tb3A in monoclinic Tb<sub>5</sub>Si<sub>2</sub>Ge<sub>2</sub> and those of P1 and Pr2 in Pr<sub>5</sub>Ge<sub>4</sub> to the same mechanism.

The proposed magnetic structure model at 9 K involves two sublattices: one consists of the Pr moments on the 4*c* sites (Pr3) and follows the Shubnikov space group  $Pn'ma'$ , and the other consists of the Pr moments on the 8*d* sites (Pr1, Pr2) and follows the Shubnikov space group  $Pnm'a'$ . This model gives a satisfactory fit to the NPD data as shown in Figs. 3(b) and 5(c). In comparison to the magnetic structure model at 30 K, the ordering of the Pr moments on the 4*c* site does not change—i.e., ferromagnetically along the *b* direction—and the atomic moment of Pr3 [ $2.66(7)\mu_B$ ] is almost the same as that at 30 K. However, the ordering on the (Pr1, Pr2) sublattice is considerably different at low temperature: the symmetry changes from  $Pn'ma'$  to  $Pnm'a'$ , the ordered moments of Pr increase to a value comparable to that of Pr3—i.e.,  $2.58(5)\mu_B$  for Pr1 and  $2.63(5)\mu_B$  for Pr2—and the principal components of the Pr1 and Pr2 mo-

ments align ferromagnetically along the *a* direction.

The change of symmetry of the magnetic structure at low temperature was also observed in the Tb<sub>5</sub>Si<sub>4</sub> compound.<sup>16</sup> The magnetic structure of Tb<sub>5</sub>Si<sub>4</sub> at 2 K was interpreted as a mixing of two magnetic modes belonging to different space groups ( $Pnm'a'$  and  $Pn'm'a'$ ). Using the combined subgroup  $P112'_1/a'$  of  $Pn'ma'$  and  $Pnm'a'$ , the refinement of the magnetic structure of Pr<sub>5</sub>Ge<sub>4</sub> at 9 K was performed with constraints on atomic position and magnetic moment to enforce pairs of Pr on the 4*e* sites to comply with the symmetry  $Pnm'a'$ . The Pr atoms on the 8*d* site (*x, y, z*) in  $Pnma$  are split into two 4*e* sites in  $P112'_1/a'$ : (*x, y, z*) and (*x, -y + 1/2, z*) with moments ( $\mu_x, \mu_y, \mu_z$ ) and ( $\mu_x, -\mu_y, \mu_z$ ), respectively, whereas the Pr on the 4*c* site in  $Pnma$  occupy the 4*e* site in  $P112'_1/a'$  with fixed  $y=1/4$  and its moment follows the  $P112'_1/a'$  symmetry. A good fit to the NPD data was achieved as shown in Fig. 5(d). The resulting magnetic structure is basically the same as the above two-sublattice model (see Table I). The main component of the Pr3 moment aligns ferromagnetically along the *b* direction with very small components on the *ac* plane. The atomic moment of the Pr3 is  $2.75(7)\mu_B$  and slightly deviates from the *b* axis with an angle of 12°. The atomic moments of Pr1 and Pr2 are  $2.64(6)\mu_B$  and  $2.69(6)\mu_B$ , respectively, and the largest components of the Pr1 and Pr2 moments align ferromagnetically along the *a* direction.

The two-sublattice model proposed for the magnetic structure of Pr<sub>5</sub>Ge<sub>4</sub> at low temperature implies that the two magnetic transitions observed in the magnetization data and the temperature dependence of the intensity of magnetic Bragg peak correspond to long-range magnetic orderings of the Pr moments on the 4*c* site and on the 8*d* sites, respectively. The Pr moments on the 4*c* site order at  $\sim 42$  K and those on the 8*d* sites at  $\sim 25$  K. The SANS data shown in

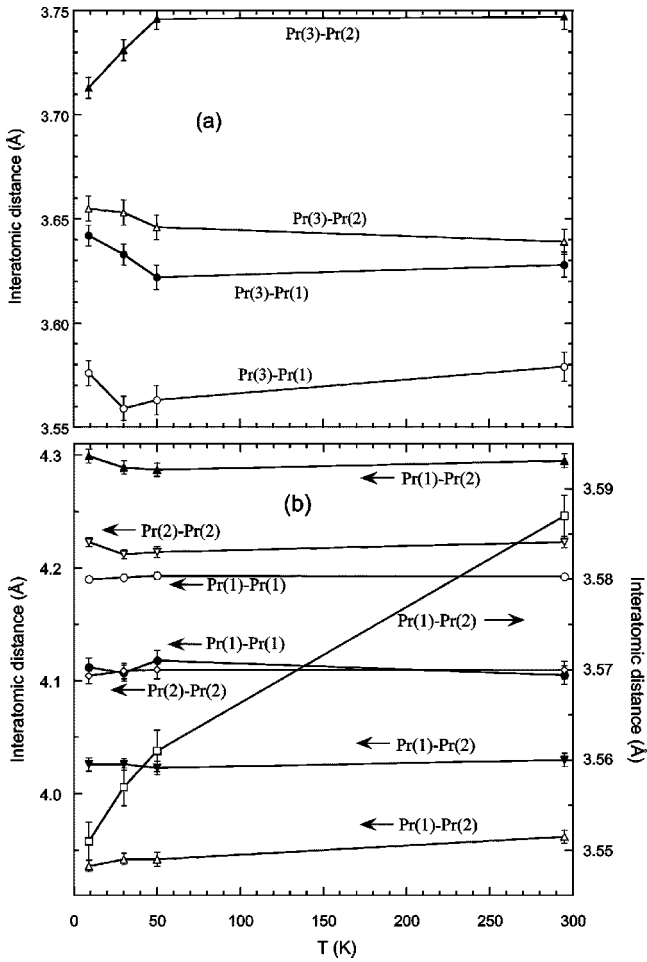


FIG. 7. The nearest Pr interatomic distances around Pr(3) (a) and distances between Pr and Pr of those at  $8d$  sites (b) as a function of temperature, indicating some changes associated with the magnetic order below 50 K.

Fig. 4(b) for  $q=0.0875 \text{ \AA}^{-1}$  exhibit two distinct peaks resulting from the critical scattering around the transition temperatures. The separate ordering of the Pr moments on different crystallographic sites can be readily understood by taking into consideration of the coordination environment of the Pr atoms in the structure. From the structural data listed in Table I, it is easy to derive that the bond length between Ge atoms at  $8d$  sites—i.e., the Ge atoms on the surface of the slabs (see Fig. 1)—does not change much and the inter-slab Ge-Ge bonds basically remain broken over the investigated temperature range, which excludes any significant contribution of the Ge-Ge bonding to the magnetic phase transitions. The magnetism of  $\text{Pr}_5\text{Ge}_4$  essentially originates from the interaction between the magnetic Pr atoms, most likely via the indirect Ruderman-Kittel-Kasuya-Yosida (RKKY) mechanism.<sup>4</sup> A Pr(3) on the  $4c$  site is coordinated by four Pr(1) and four Pr(2) atoms on the  $8d$  sites, forming a distorted body-centered cube. The interatomic distance from the center atom Pr(3) to Pr(1) and Pr(2) ranges from 3.574 to 3.713 Å at 9 K. Figure 7 shows the Pr-Pr interatomic distances ( $<4.3 \text{ \AA}$  only) as a function of temperature. The distances of three ligand Pr atoms—two on the  $4c$  site [Pr(3)]

and one on the  $8d$  site [Pr(2) or Pr(1)]—to the center Pr atom on the  $8d$  site [Pr(1) or Pr(2)] are obviously shorter than those of other ligand Pr atoms [Pr(1) or Pr(2)], leading to a much longer average Pr-Pr distance for the Pr atoms on the  $8d$  sites.<sup>18</sup> The shortest Pr(1)-Pr(2) distance corresponds to the one interconnecting two Pr slabs as indicated in Fig. 1. It seems the ordering of Pr3 increases the Pr3-Pr1 and Pr3-Pr2 distances due to the magnetostriction and reduces the Pr1-Pr2 distance accordingly. The salient difference in the coordination environment of the Pr atoms on the  $4c$  site and on the  $8d$  sites should be responsible for the different ordering temperatures of the Pr moments on the two sublattices.

It is noteworthy that the easy magnetization direction of the Pr moments on the  $4c$  site is along the  $b$  axis and is different from that in other reported  $R_5\text{Ge}_4$  compounds,<sup>13-17</sup> in which the easy magnetization direction of the  $R$  moments on the  $4c$  site is perpendicular to the  $b$  axis. Considering that the reported  $R_5\text{Ge}_4$  compounds crystallize in different magnetic space groups depending on the nature of the rare earth, it is speculated that the electron configuration of the rare earth metals may play a critical role for the  $R_5\text{Ge}_4$  compounds to adopt the specific magnetic structures (Pr:  $[\text{Xe}]4f^36s^2$ ; Nd:  $[\text{Xe}]4f^46s^2$ , Tb:  $[\text{Xe}]4f^96s^2$ ; Ho:  $[\text{Xe}]4f^{11}6s^2$ ). Phenomenologically, the anisotropy of the rare earth metal sublattice is essentially determined by the first-order anisotropy constant  $K_1$ , which is derived as

$$K_1 = -\frac{3}{2}A_{20}\alpha_J\langle r^2 \rangle \langle O_{20} \rangle - 5A_{40}\beta_J\langle r^4 \rangle \langle O_{40} \rangle - \frac{21}{2}A_{60}\gamma_J\langle r^6 \rangle \langle O_{60} \rangle,$$

where  $A_{20}$ ,  $A_{40}$ , and  $A_{60}$  are crystal-field coefficients determined only by the crystallographic type,  $\alpha_J$ ,  $\beta_J$ , and  $\gamma_J$  are Stevens factors independent of the crystal structure, and the terms  $\alpha_J\langle r^n \rangle \langle O_{n0} \rangle$ , etc., are characteristics of the rare earth ions. The second- and fourth-order Stevens factors  $\alpha_J$  and  $\beta_J$  are comparable negative values for  $\text{Pr}^{3+}$ ,  $\text{Nd}^{3+}$ ,  $\text{Tb}^{3+}$ , and  $\text{Ho}^{3+}$ , whereas the sixth-order Stevens factors  $\gamma_J$  for these rare earth ions are distinctly different:  $60.99 \times 10^6$ ,  $-37.99 \times 10^6$ ,  $-1.212 \times 10^6$ , and  $-1.294 \times 10^6$  for  $\text{Pr}^{3+}$ ,  $\text{Nd}^{3+}$ ,  $\text{Tb}^{3+}$ , and  $\text{Ho}^{3+}$ , respectively.<sup>23</sup> Therefore, higher-order terms of the crystal field could be responsible for the observed magnetic structures of the  $R_5\text{Ge}_4$  compounds for different rare earth elements.

#### IV. CONCLUSIONS

Small-angle neutron scattering and neutron powder diffraction experiments reveal that there are two magnetic phase transitions in the  $\text{Pr}_5\text{Ge}_4$  compound at  $\sim 25 \text{ K}$  and  $\sim 42 \text{ K}$ , respectively, consistent with low-field magnetization measurements.<sup>18</sup> Refinements of the magnetic structures based on high-resolution neutron diffraction data indicate that the magnetic phase transitions originate from the long-range orderings of the Pr moments on the  $4c$  site and on the  $8d$  sites, respectively. Between these two transitions the

magnetic structure belongs to the space group  $Pn'ma'$  with small induced Pr moments on the  $8d$  sites. Below 25 K, the magnetic structure consists of two magnetic sublattices: one on the  $4c$  sites with  $Pn'ma'$  symmetry, the other on the  $8d$  sites with  $Pnm'a'$  symmetry. However, the crystal structure retains the  $Pnma$  symmetry over the investigated temperature regime (1.5–300 K). The separate ordering of the Pr moments on different crystallographic sites can be readily understood by the salient difference in the rare earth metal environments around different crystallographic sites. In contrast to other reported  $R_5\text{Ge}_4$  compounds, the Pr moments on

the  $4c$  site in Pr<sub>5</sub>Ge<sub>4</sub> align along the  $b$  axis, which can be attributed to the contribution of higher-order terms of the crystal field to the magnetocrystalline anisotropy of  $R_5\text{Ge}_4$  compounds.

#### ACKNOWLEDGMENT

This work was supported by the National Natural Science Foundation of China, the State Key Project of Fundamental Research, the National “863” project, and the exchange program between NIST and the Chinese Academy of Sciences.

- 
- <sup>1</sup>V.K. Pecharsky and K.A. Gschneidner, Jr., Phys. Rev. Lett. **78**, 4494 (1997).  
<sup>2</sup>V.K. Pecharsky and K.A. Gschneidner, Jr., Appl. Phys. Lett. **70**, 3299 (1997).  
<sup>3</sup>L. Morellon, P.A. Algarabel, M.R. Ibarra, J. Blasco, B. Garcia-Landa, Z. Arnold, and F. Albertini, Phys. Rev. B **58**, R14 721 (1998).  
<sup>4</sup>W. Choe, V.K. Pecharsky, A.O. Pecharsky, K.A. Gschneidner, Jr., V.G. Young, Jr., and G.J. Miller, Phys. Rev. Lett. **84**, 4617 (2000).  
<sup>5</sup>E.M. Levin, V.K. Pecharsky, and K.A. Gschneidner, Jr., Phys. Rev. B **60**, 7993 (1999).  
<sup>6</sup>K.A. Gschneidner, Jr., V.K. Pecharsky, A.O. Pecharsky, V.V. Ivchenko, and E.M. Levin, J. Alloys Compd. **303–304**, 214 (2000).  
<sup>7</sup>L. Morellon, C. Magen, P.A. Algarabel, M.R. Ibarra, and C. Ritter, Appl. Phys. Lett. **79**, 1318 (2001).  
<sup>8</sup>D.H. Ryan, M. Elouneq-Jamroz, J. von Lierop, Z. Altounian, and H.B. Wang, Phys. Rev. Lett. **90**, 117202 (2003).  
<sup>9</sup>G.S. Smith, A.G. Tharp, and Q. Johnson, Acta Crystallogr. **22**, 940 (1967).  
<sup>10</sup>F. Holtzberg, R.J. Gambino, and T.R. McGuire, J. Phys. Chem. Solids **28**, 2283 (1967).  
<sup>11</sup>V.K. Pecharsky and K.A. Gschneidner, Jr., Adv. Mater. (Weinheim, Ger.) **13**, 683 (2001).  
<sup>12</sup>W. Choe, V.K. Pecharsky, A.O. Pecharsky, K.A. Gschneidner, Jr., V.G. Young, Jr., and G.J. Miller, Phys. Rev. Lett. **84**, 4617 (2000).  
<sup>13</sup>P. Schobinger-Papamantellos, J. Phys. Chem. Solids **39**, 197 (1978).  
<sup>14</sup>P. Schobinger-Papamantellos and A. Niggli, J. Phys. (Paris), Colloq. **40**, C5-156 (1979).  
<sup>15</sup>P. Schobinger-Papamantellos and A. Niggli, J. Phys. Chem. Solids **42**, 583 (1981).  
<sup>16</sup>C. Ritter, L. Morellon, P.A. Algarabel, C. Magen, and M.R. Ibarra, Phys. Rev. B **65**, 094405 (2002).  
<sup>17</sup>J.M. Cadogan, D.H. Ryan, Z. Altounian, H.B. Wang, and I.P. Swainson, J. Phys.: Condens. Matter **14**, 7191 (2002).  
<sup>18</sup>H.F. Yang, G.H. Rao, G.Y. Liu, Z.W. Ouyang, X.M. Feng, W.F. Liu, and J.K. Liang, Phys. Status Solidi A **198**, 156 (2003).  
<sup>19</sup>H.F. Yang, G.H. Rao, W.G. Chu, G.Y. Liu, Z.W. Ouyang, and J.K. Liang, Alloys Compd. **339**, 189 (2002).  
<sup>20</sup>A.C. Larson and R.B. von Dreele (unpublished).  
<sup>21</sup>J.W. Lynn, L. Vasiliu-Doloc, and M.A. Subramanian, Phys. Rev. Lett. **80**, 4582 (1998).  
<sup>22</sup>L. Morellon, C. Ritter, C. Magen, P.A. Algarabel, and M.R. Ibarra, Phys. Rev. B **68**, 024417 (2003).  
<sup>23</sup>H.S. Li and J.M.D. Coey, in *Handbook of Magnetic Materials*, edited by K.H.J. Buschow (North-Holland, Amsterdam, 1991), Vol. 6, p. 1.